Pergamon

Int. J. Heat Mass Transfer. Vol. 41, No. 14, pp. 2143–2155, 1998

Printed in Great Britain
0017–9310/98 $19.00+0.00

PII: S0017–9310(97)00344–X

Terrestrial and microgravity pool boiling heat transfer from a wire in an acoustic field

J. S. SITTER, T. J. SNYDER and J. N. CHUNG†
School of Mechanical and Materials Engineering

and

P. L. MARSTON
Department of Physics, Washington State University, Pullman, WA 99164, U.S.A.

(*Received* 18 *November* 1996 *and in final form* 4 *November* 1997)

Abstract—Pool boiling heat transfer experiments from a platinum wire heater in FC-72 liquid were conducted under terrestrial and microgravity conditions, both with and without the presence of a high intensity acoustic standing wave within the fluid. The purpose of this research was to determine the effects of an acoustic sound field on nucleate pool boiling in both terrestrial gravity and microgravity. The platinum wire heater was used as a constant heat flux source and as a thermometer. The effects of acoustics on heat transfer were measured by the change in the average surface temperature of the heater. In terrestrial gravity a partial boiling curve was established with and without acoustics. In general, it was found that both the natural convection and boiling heat transfer rates were increased with the presence of an acoustic standing wave in terrestrial gravity. The highest heat transfer augmentation was registered when the heater wire was placed at the acoustic pressure antinode. In microgravity, the acoustic force was shown to be a promising means in maintaining nucleate boiling. © 1998 Elsevier Science Ltd. All rights reserved.

1. INTRODUCTION

The exploration of space by the space shuttle and space lab has created many engineering problems. Many of these problems stem from the loss of buoyancy force due to the lack of gravity. Therefore, the vapor bubble dynamics in pool boiling is considerably different in microgravity from that in terrestrial gravity. In space the vapor bubbles tend to remain attached or stay in close proximity of the heater surface. Thus, film boiling and burnout can occur in microgravity at heat fluxes much lower than those required on earth. A stable heat transfer process in space will be required as needs for transferring heat effectively, efficiently, and safely grow with increasing space activities. This paper addresses the feasibility of using acoustics to maintain efficient boiling in microgravity.

Pool boiling in an acoustic field is very complex due to a myriad of mechanisms occurring simultaneously. To date no research has been found in the literature on the effects of an acoustic standing wave on pool boiling heat transfer in microgravity. The current study examines and elucidates about the effects of using a high intensity sound field during pool boiling from a platinum wire heater in FC-72 under terrestrial and microgravity conditions. This is accomplished by measuring the change in the average surface temperature of the heater going from terrestrial gravity into microgravity and the effects due to acoustics. Video images of vapor bubble dynamics under various heat fluxes, acoustic pressure amplitudes, heater positions within the sound field, and also gravity conditions are presented to aid in the analysis.

The specifics of the research involved investigating the interaction between pool boiling heat transfer and the sound field. Previous research has shown that a sound field can increase the heat transfer coefficient in certain pool boiling regimes [1]. Mainly acoustic cavitation has been cited as the main mechanism for augmenting the heat transfer coefficient [2]. Thus, some of the intrinsic effects of a high pressure acoustic standing wave are suspected to also increase heat transfer during microgravity. These effects include cavitation, streaming, vapor bubble oscillations, dynamic vapor bubble levitation and erratic dancing of bubbles. The manifestation of the acoustic effects mentioned here and others can alter and even control vapor bubble movement and growth.

The experiment looked specifically into the following pool boiling–acoustics interaction phenomena in both terrestrial and microgravity conditions:

1. The effects of changing the acoustic pressure amplitude on pool boiling heat transfer.
2. The importance of heater position within the acoustic standing wave.

† Author to whom correspondence should be addressed.

3. The elimination of thermal overshoot at the inception of boiling in terrestrial gravity due to acoustic cavitation.

2. LITERATURE REVIEW

2.1. *Pool boiling in microgravity*

Straub *et al.* [3] states that the first experiments performed in microgravity contradicted each other. These experiments were usually conducted in drop towers in which microgravity times were less than 4 s. It was assumed that these drop times were too short for transients to settle. There is a problem with either turning on a heater before or during a drop. If turned on before the drop, transient convection can exist. If the heater is turned on during the drop and high heat fluxes are needed to boil, an unstable transition to film boiling could occur.

Pool boiling in terrestrial and microgravity are dependent on the heater geometry. Thus, a wire heater and a flat plate will affect the departure diameter of the vapor bubbles in different ways. This can be contributed to the contact perimeter of the bubble on the heater surface.

The most interesting part of the paper is the section entitled, 'The Mechanism of Boiling'. This section discusses different pool boiling conditions, saturated liquid state, subcooled liquid state, critical heat flux, and film boiling. It is noted by Straub *et al.* [3] that evaporation and surface tension effects are the basic mechanisms in microgravity. While in terrestrial gravity, buoyancy is the governing mechanism for boiling heat transfer.

Eastman [4] goes over the forces acting on a bubble in terrestrial gravity and states that the forces that hold the bubble to the heater surface are surface tension and form drag. The forces that pull the vapor bubbles off the surface are internal pressure, inertia, and buoyancy. Without buoyancy, inertia and the internal pressure of the vapor bubble can still overcome surface tension. Eastman notes that form drag is negligible compared to the other forces. It was noted that the vapor bubble does not have a large inertia but the fluid around the bubble does. Thus, with quick bubble growth the fluid around the bubble has enough inertia to pull the bubble off the heater surface during microgravity. Eastman notes that inertia is the prominent force for lifting bubbles off a heated surface when the buoyancy force is not present.

Weinzierl and Straub [5] found that for pool boiling at low heat fluxes the heat transfer coefficient is equal to or higher in microgravity than in terrestrial gravity. This is because the inception of boiling occurred at lower heat fluxes in microgravity. They attest that a heat transfer mechanism exists that appears to be independent of gravity. A mechanism noted in the paper that is responsible for transferring a larger amount of heat is evaporation and condensation of liquid around a vapor bubble. Evaporation takes place on the lower part of the bubble closest to the heater. The condensation takes place at the top of the bubble which is the farthest from the heater.

2.2. *Effects of acoustics on heat transfer*

The effects of ultrasonics on pool boiling heat transfer were discussed by Park and Bergles [6]. The experimental setup consisted of a modified ultrasonic cleaning tank with R-113 as the working fluid. The experiments were run with saturated and subcooled fluid. They state that the position of the heater in the acoustic field did not have any noticeable effects on the heat transfer curve under saturated conditions. However, the acoustic pressure amplitude did. It was also noted that at moderate heat fluxes, heat transfer decreased. At higher heat fluxes acoustics had minimal effects on the heat transfer curve. These effects were thought to be caused by the development of large amounts of vapor around the heater. As the heat flux was increased more vapor was produced as with the increase of acoustic pressure. Thus, the highest increase in heat transfer was at low heat fluxes and when the fluid was subcooled.

Wong and Chon [1] found that there is a critical sound pressure CSP below which there is no effect on the boiling heat transfer curve. A 800% increase in heat transfer coefficient was found in the natural convection regime. In the fully developed nucleate boiling regime, acoustics had a negligible effect on the heat transfer coefficient. The reason for the increase in heat transfer was thought to be the erratic motion of bubbles and the radial oscillations of the bubbles in the vicinity of the heater surface. Changing the driving frequency of the system was found to have negligible effect so long as the same amount of cavitation was maintained.

Iida *et al.* [2] found that acoustics had minimal heat transfer effects on nucleate boiling but did affect the natural convection and film boiling regimes. The maximum and minimum heat flux points were raised. The driving mechanism for increasing heat transfer was thought to be mainly acoustic cavitation.

3. THEORETICAL BACKGROUND

In pool boiling under terrestrial gravity the buoyancy force of a vapor bubble is larger than the gravitational force thus, the bubbles rise. The buoyancy force (F_b) is large enough to pull vapor bubbles off the heater and through liquid. Then if a force can be found that is equal to or greater than the F_b, that force should then be strong enough to maintain nucleate boiling during microgravity. The use of acoustics to overcome the buoyancy force of air bubbles and oil droplets in water in shown in [7–9].

3.1. *Force balance*

The acoustic force of a standing wave on a bubble is given by the following equations [10]:

$$Fa = -\langle V(t)\nabla p_a(\mathbf{r}, t)\rangle \quad (1)$$

$$Fa = -\frac{2\pi^2 R^3 Pa^2}{3Po\lambda_z\beta\left(1-\frac{\omega^2}{\omega_0^2}\right)}\sin\left(\frac{4\pi z}{\lambda_z}\right) \quad (2)$$

$$Fa = Fb - Fg = Vo(\rho_l - \rho_v)g \quad (3)$$

where $V(t)$ is the volume of the bubble which changes with time, p_a is the acoustic pressure which changes with time and position, R is the equilibrium radius of the bubble, Pa is the acoustic pressure amplitude, Po is atmospheric pressure plus hydrostatic pressure, β is the polytropic exponent and is equal to 1.4 if oscillations are adiabatic, λ_z is the wavelength in the z direction, ω and ω_0 are the natural frequencies of the sound field and bubble, respectively. ρ_l and ρ_v are the densities of the liquid and vapor phases, respectively. The brackets in equation (1) denotes the average over one period of the sound wave. It is noted, however, that the vapor bubble's natural frequency is based on the following equation:

$$\omega_0^2 = \left(\frac{3\beta Po}{\rho_l R^2}\right). \quad (4)$$

The acoustic force on a vapor bubble presented here does not include the effects of evaporation, condensation [7] and damping [8], which are of minor importance for the frequency range in the current research.

From equation (1) it can be seen that the acoustic force on a bubble is a time averaged force. The acoustic force depends on the acoustic pressure amplitude, bubble size, and the driving frequency of the system. The driving frequency, the pressure amplitude and the bubble size will determine the bubble dynamics and movement. It should be noted that equation (2) is based on a plane standing wave in the z direction. By setting equation (2) equal to (3) one can solve for the acoustic pressure amplitude [see equation (5)].

$$Pa^2 = \frac{2g\lambda_z\beta(\rho_l - \rho_v)\left(1-\frac{\omega^2}{\omega_0^2}\right)}{\pi\sin\left(\frac{4\pi z}{\lambda_z}\right)}. \quad (5)$$

3.2. *Levitation positions in microgravity*

Looking at equation (2) it can be seen that the sign for Fa depends on where the bubble is located in the sound field and the size of the bubble, Fig. 1. In the absence of any other force fields if the bubbles are smaller than resonance size the bubbles migrate toward the pressure antinodes. If the bubbles are larger than resonance size the bubbles migrate toward the pressure nodes. Most vapor bubbles are larger than resonance size. The bubbles that are smaller than resonance size tend to coalesce at the antinode then grow larger and propagate toward the pressure node.

4. EXPERIMENTAL SETUP

An experimental apparatus was built to study the effects of high intensity sound pressure on pool boiling in both terrestrial and microgravity environments. The experiment was mounted in a rig designed to fit in either the 0.6 or 2.1 s drop tower at WSU. The apparatus has the dimensions of 16″ × 16″ × 16.5″ with a weight of approximately 50 lbs.

4.1. *Experimental layout*

The acoustic and pool boiling system consists of the following components: the acoustic resonator, the fluid chamber, the base of the fluid chamber, and a platinum wire heater (Fig. 2). A DC power supply, computer with an A/D card, frequency generator, and an acoustic amplifier are connected to the experiment by a series of shielded electrical wires with quick-disconnect plugs. The experiment is housed in a rig. Details on the acoustic fluid chamber, acoustic resonator, platinum wire heater, heater calibration, average heater surface temperature measurement, video camera system, and experimental rig are provided in Sitter [11].

4.2. *Experimental fluids*

FC-72 Fluorinert liquid supplied from 3M company was used for the heat transfer experiments. FC-72 has some advantages (1, 2, 3) and disadvantages (4, 5):

1. Highly dielectric, an excellent electrically insulating fluid.
2. Non-toxic and non-flammable.
3. Low boiling point ~56°C under atmospheric condition.
4. Low speed of sound ~1/3 of water.
5. The ability to absorb large amounts of air (affinity for air).

4.3. *Data acquisition system*

The data acquisition system contains a 486 PC, A/D board, and a program called 'Pulse'. Pulse is a Windows based program that reads the data in from the A/D card. The data acquisition system has several input channels and has one output channel. The input channels were used for measuring the power input to the heater. The output channel is used to switch on a relay which turns on a solenoid that knocks out a tapered pin to release the experimental rig into microgravity.

4.4. *Microgravity facility*

Three functional drop towers are available at WSU. Two of them have microgravity times of 0.6 s, the third has a microgravity time of 2.1 s. The 0.6 and 2.1 s drop towers used in this experiment employ an air bag as a deceleration mechanism. The average microgravity levels are 5×10^{-3} and 5×10^{-4} a g^{-1} for the 0.6 and 2.1 s drop towers, respectively. It is

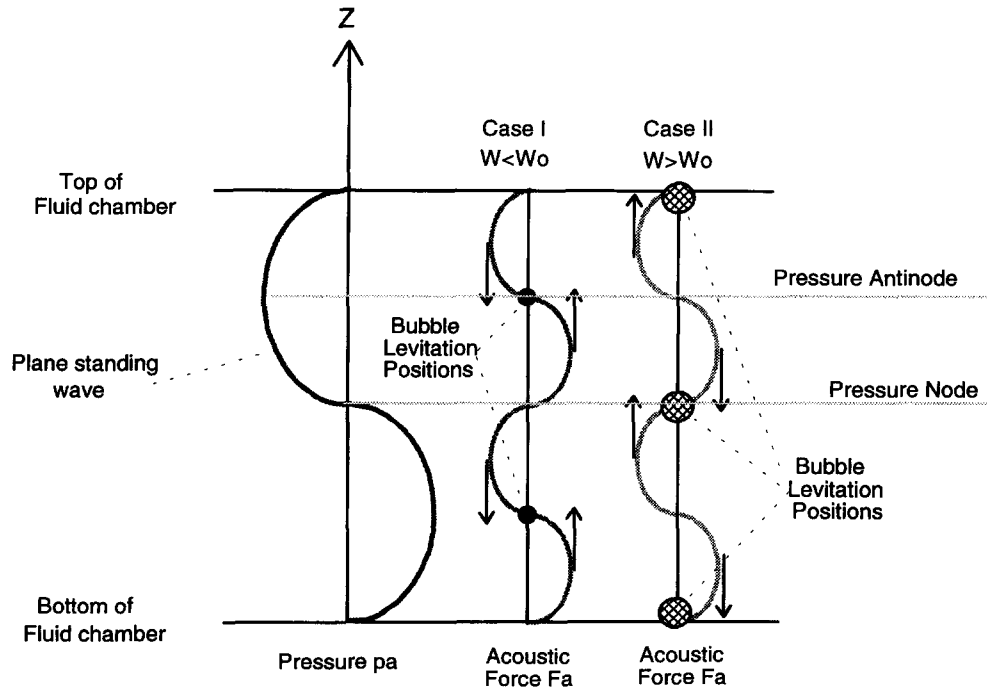

Fig. 1. Bubble levitation positions in an acoustic plane standing wave.

important to clarify that both the 0.6-s and 2.1-s drop towers provided enough microgravity time for our study. Cooper *et al.* [12] gave an experimentally verified formula for predicting bubble life time (from nucleation to detachment from the heater surface) under normal gravity. For FC-72, we estimated that two to eight bubble cycles are possible between 0.6 to 2.1 s. Since the acoustic force strengths in our experiment (1.5 and 2.6 atm) are comparable to that of gravity, we believe that the microgravity time was adequate for the results. Pool boiling in microgravity without an external force field would require much longer time and therefore, drop towers usually do not provide enough time as mentioned in the literature review section.

5. EXPERIMENTAL PROCEDURE

5.1. *Coupling the acoustic resonator with the fluid chamber*

The actual natural frequency of the acoustic resonator and the fluid chamber do not follow the theories exactly. The theories did give a good estimate for a starting point.

The resonator was machined for a frequency which was slightly lower than desired. Thus the resonator was too long. The resonator's natural frequency was then checked with an electrical impedance meter and then remachined incrementally until its desired natural frequency was obtained.

The fluid chamber was built following the theoretical equations. However, the chambers height was constructed longer than needed to allow for fluid height adjustment. The resonator was constructed and installed with the fluid chamber, then the fluid height was adjusted. The fluid level was adjusted for the highest acoustic pressure amplitude, and the cleanest sinusoidal pressure distribution in the vertical direction. The pressure was measured with a hydrophone.

5.2. *Calibration of the hydrophone and resonators*

The hydrophone was calibrated by the technique described by Crum [9]. The acoustic pressure amplitude required to levitate a droplet in a fluid is given by the following equation:

$$Pa = \left(\frac{4|1-\delta|g\rho_l^2 c^2}{k_z \left[\left(\frac{1}{\delta \sigma_v^2} \right) - \left(\frac{5\delta - 2}{2\delta + 1} \right) \right]} \right)^{0.5} \tag{6}$$

where Pa is the acoustic pressure amplitude, k_z is the wave number in the vertical direction z, ρ_l is the density of the fluid, σ_v is the velocity ratio, c is the speed of sound in the medium, and δ is the ratio of density of the droplet to the density of the fluid medium. The hydrophone was calibrated using the 5.08 cm diameter resonator coupled to the water-filled chamber. The hydrophone was submerged in the water, the fluid height was then adjusted to maximize the voltage out-

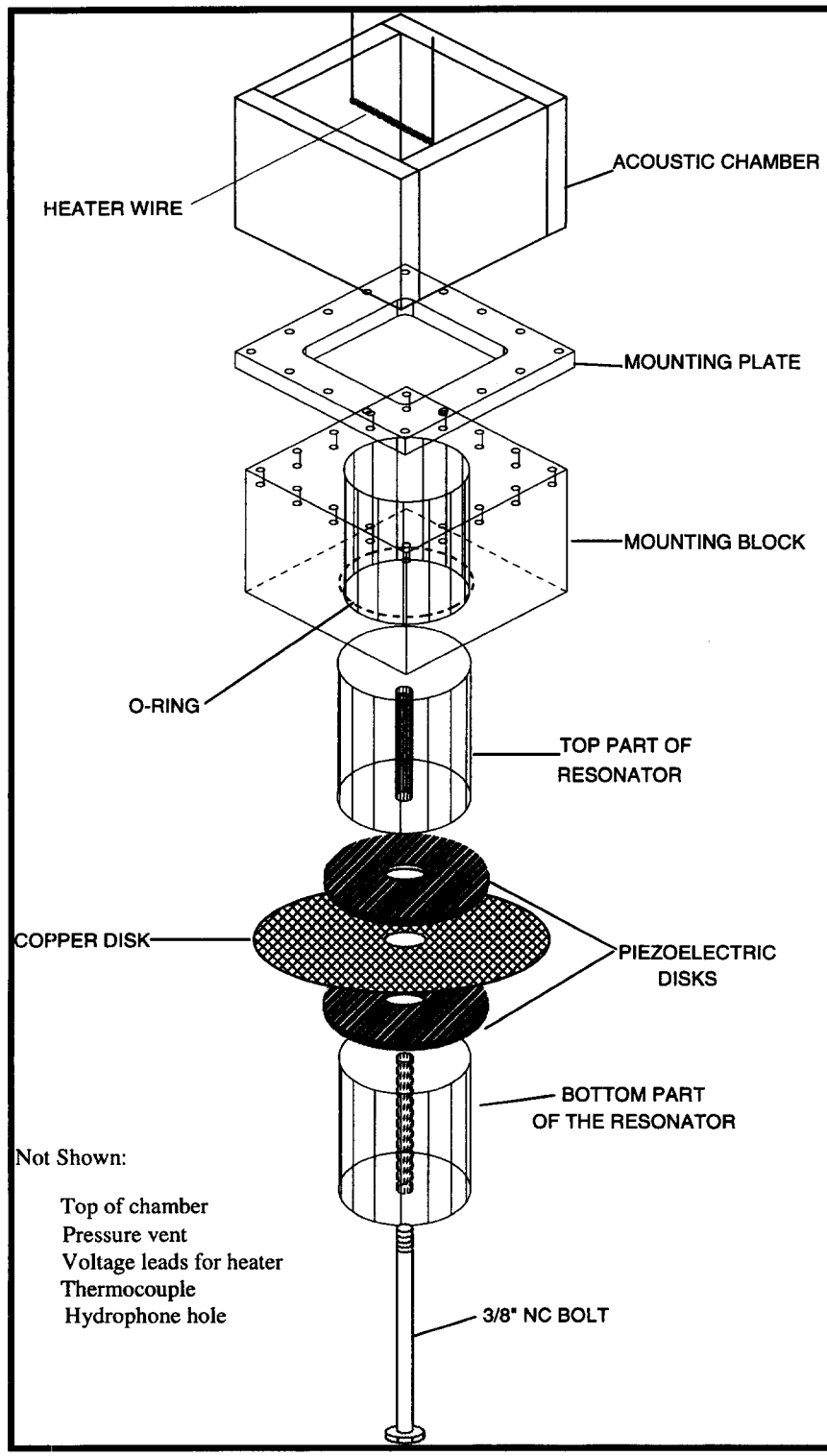

Fig. 2. Exploded view of the experimental setup for pool boiling in an acoustic pressure field under terrestrial and microgravity conditions.

put of the hydrophone for a set output pressure from the resonator. The correct fluid height maximized the coupling between the resonator and the fluid filled chamber. A vertical pressure scan was then performed. The hydrophone was removed from the water chamber and set aside. The voltage to the resonator

was turned up as high as possible. A silicon oil droplet was then injected into the water below a pressure antinode. The droplet rose in the fluid until the acoustic force balanced the buoyancy force. The voltage to the resonator was then turned down incrementally until the droplet's buoyancy overcame the acoustic force and it rose to the water surface. The voltage to the resonator was then recorded. Two different droplets were levitated, 20 centiStoke and 100 centiStoke Dow Corning 200 series silicon fluids. Equation (6) was then used to find the acoustic antinode pressure required to levitate the 100 centiStoke droplet. Then a single point calibration was used to find the pressure required to levitate the 20 centiStoke droplet. The percent difference between the measured and the extrapolated value was 0.25%. The driving frequency of the resonator was 27.4 kHz and the fluid height in the chamber was 7.2 cm. The value for k_z was found by using the relationship $k_z = 2\pi/\lambda_z$ and the wavelength in the z direction was found by doing a vertical pressure scan with the hydrophone.

The voltage input to the 5.08 cm resonator was set to an amplitude that the hydrophone could read. The hydrophone was inserted into the water. The voltage to the resonator was then raised incrementally and the voltage output of the hydrophone was recorded. A linear relationship between the resonator voltage input and hydrophone voltage output was found. Knowing the resonator–hydrophone relationship and the resonator–pressure relationship allowed determining a hydrophone–pressure relationship. Using these relationships, the hydrophone output in terms of pressure was found as:

$$Pa(\text{atm}) = 4.5125*\text{hydro(V)} - 0.00012 \qquad (7)$$

where Pa(atm) is the acoustic antinode pressure in atmospheric gauge pressure and hydro(V) is the hydrophone output in volts.

The hydrophone was inserted into the FC-72 fluid chamber which uses the 7.62 cm resonator. The fluid height was determined based on obtaining the best standing wave. A vertical pressure run was also carried out. The voltage to the 7.62 cm resonator was increased incrementally and the voltage output of the hydrophone was recorded. Thus, a linear relationship between the voltage input to the resonator vs pressure output into the fluid by the resonator was found. The driving frequency of the 7.62 cm resonator was 10.18 kHz, with a fluid height of 7.2 cm.

Once the fluid height for the FC-72 chamber was known, the sides of the chamber were machined and a 1/4″ plexiglass top was attached to the walls. The total height of the chamber was then 7.2 cm. Five holes were machined in the top of the chamber. Two holes for the heater, one for a vapor vent and fluid fill hole, another for a thermocouple, and the last hole was used to take pressure measurements with the hydrophone. The hydrophone was then inserted through a 0.32 cm pipe hole on the top of the chamber to measure the pressure in the chamber.

5.3. *Degassing FC-72*

The FC-72 was degassed by several different processes: boiling by heating, boiling by drawing a vacuum, and by acoustic cavitation. The most efficient was found by drawing a vacuum. All three worked but drawing a vacuum was the quietest, fastest, and safest. Boiling the fluid by heating meant that the fluid had to be cooled before it could be used for the experiment. The fluid during the cool down process would reabsorb air. A large amount of fluid would evaporate during heating and thus, the processes took over 10 min. Using acoustics to cavitate the fluid was noisy and took under 10 min. When drawing a vacuum, the fluid would instantaneously boil and would be degassed within 3 min, and the process was fairly quiet.

5.4. *Positioning the heater*

Once the fluid was in the chamber and degassed the voltage to the resonator was raised until heavy cavitation was present. The creation of vapor bubbles at the acoustic pressure antinode and node was visible. Large vapor bubbles were seen to be levitated at the node until they grew too large. The heater position could then be established by seeing the pressure nodes and antinodes. This visual positioning of the antinode and node was checked with the hydrophone and was determined to be accurate.

5.5. *Average heater surface temperature*

The average heater surface temperature, was converted from the resistance reading during the experiment. With the following equation:

$$T = \frac{dT}{dR} R_r + b \qquad (8)$$

dT/dR is the slope from the heater calibration curve and b is from the single point calibration, R_r is the resistance reading taken during the experiment.

5.6. *Heat flux*

The heat flux from the heater was calculated with the equation:

$$q = \frac{V*I}{A_s} \qquad (9)$$

where V is the voltage drop across the heater, A_s is the surface area of the heater, and I is the current that is flowing through the heater. The current is determined by a voltage drop across a resistor $I = V/R$. The voltages were measured by the A/D card.

5.7. *Bulk temperature of the fluid*

The bulk temperature of the fluid was measured with a copper–constantin thermocouple. To ensure that stratifications within the fluid were eliminated before each experimental run the acoustic pressure field was raised, producing acoustic streaming. The strong mixing produced by the acoustic streaming

brought the fluid to one temperature. The acoustics were turned off and the fluid was allowed to rest until all signs of fluid motion disappeared.

6. RESULTS

6.1. *Experimental conditions and uncertainties*

The research was broken down into two parts. The first part consisted of creating partial boiling curves with and without acoustics under terrestrial gravity conditions (bench top experiment). The second part was performed in the 0.6-s and 2.1-s drop towers at Washington State University. Different heat fluxes were set and the average surface temperature was measured with and without acoustics in both terrestrial condition and microgravity. All experiments were conducted under atmospheric pressure which corresponded to a saturation temperature of 54.5°C for FC-72. The resonators driving frequency was always set at 10.18 kHz. The acoustic pressure amplitude was 2.6 atm gauge unless otherwise stated. One of the difficulties experienced during the experiment is the rise in bulk temperature of the fluid under high heat flux conditions. Therefore, the experiment was allowed to cool between runs and the fluid level was raised to the correct level with clean degassed FC-72. The resonance of the fluid chamber changed with temperature and fluid height. Thus, with a change of 1 mm in fluid height or a few degrees in fluid temperature the acoustic chamber can be detuned by 1000 kHz. In pool boiling, the creation of vapor bubbles also further detuned the acoustic chamber. For these reasons precise resonance frequency and acoustic pressure amplitude were not known because they were continually changing during each experiment. However, an error analysis showed measurement uncertainties of $\pm 5.613 \times 10^{-4}$ ohm for heater resistance, ± 1.312°C for temperature, ± 0.0249 W cm^{-2} for heat flux, and ± 0.04345 W cm^{-2} K for heat transfer coefficient. The details of the uncertainty analysis are given in Sitter [11].

6.2. *Results from the bench top experiment*

The data from the bench top experiments were used to create the boiling heat transfer curves with and without acoustics. The heat flux was varied from pure conduction on through the isolated bubble regime. Critical heat flux was avoided initially because the transition to burnout would happen suddenly and the destruction of the heater was a concern. Thus, once the heat transfer curves were established the higher heat fluxes were attempted.

Figures 3 and 4 contain the same data but are presented two different ways. These figures are confined to heat fluxes from 0 to 24 W cm^{-2}. Figure 3 is a standard boiling curve and is presented with heat flux vs degree of superheat for the heater. The heat flux is measured as $q = V^*I/S_a$, with $q =$ W cm^{-2}, $V =$ volts across the heater, $I =$ amps through the heater, and $S_a =$ surface area of the heater. The degree of superheat is defined as the difference in temperatures between the temperature of the heater and saturation temperature of the fluid. It can be seen in Fig. 3 that the heat transfer curves are naturally grouped into three sections. The first section is normal pool boiling without the effects of acoustics. The second section is pool boiling with acoustics and the heater located at the acoustic pressure node. The third section is pool boiling with acoustics and the heater placed at the acoustic pressure antinode.

In Fig. 4, for heat transfer data without acoustics the correlation from Churchill and Chu correlation [13] is presented for the natural convection data. In the nucleate boiling regime the Stephan and Abdelsalam correlation [14] was used to compare with the experimental data. The close agreement between the current data and both correlations ensured that the experiment system performed correctly.

Figure 5 shows the effect of a sound field on the heater surface temperature under a constant heat flux of 33.2 W cm^{-2} when acoustics was implemented. At the heat flux of 33.2 W cm^{-2}, boiling was in the isolated bubble regime (Fig. 5).

6.3. *Results from experiments in the drop tower*

To get both terrestrial and microgravity results in the drop tower, the heater was turned on before the rig was dropped. The data acquired in this section are based on surface temperature measurement as the heat flux was held constant and the following system conditions: heater placed at different positions within the sound field (for example, pressure antinodes and nodes), pool boiling with and without acoustics.

A typical graph of heater temperature vs time is given in Fig. 6. The graph is based on a constant heat flux of 3.98 W cm^{-2}. Data obtained for Figs. 5 and 6 and other cases of different heat fluxes are summarized in Table 1.

7. DISCUSSION OF RESULTS

The effects of acoustics on the heat transfer and vapor bubble movement in pool boiling depend on many factors. The properties of the experiment that can be controlled were the heat flux, acoustic pressure amplitude, heater position within the sound field, and the gravity level.

7.1. *Terrestrial gravity*

7.1.1. *Heater position.* The placement of the heater within the sound field was found to be critical, see Fig. 3. The heater was placed at several positions within the sound field. Special attention was given to the following heater positions within the sound field: pressure node, pressure antinode, and halfway between the pressure node and antinode where the acoustic force in theory is the highest. The heat transfer increased for a given degree of superheat when the heater was positioned anywhere within the sound field. However, the heat transfer had the highest

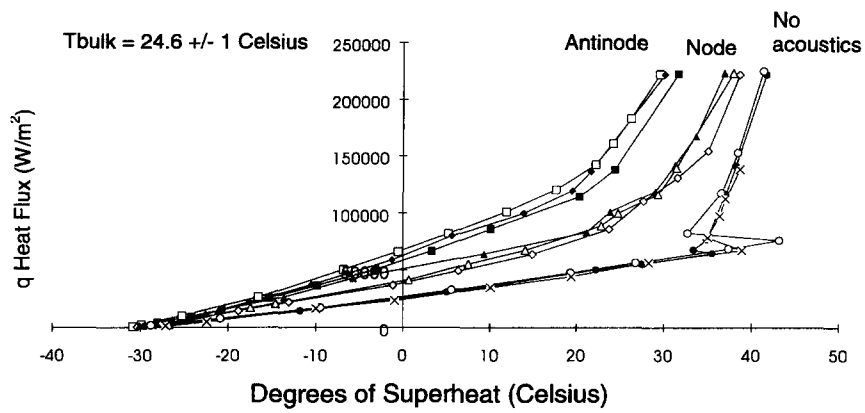

Fig. 3. Heat transfer curve for FC-72 with a platinum wire heater in an acoustic sound field.

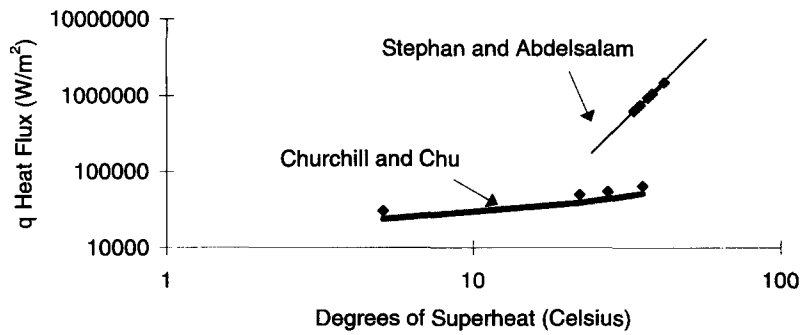

Fig. 4. Heat transfer curve for FC-72 with a platinum wire heater.

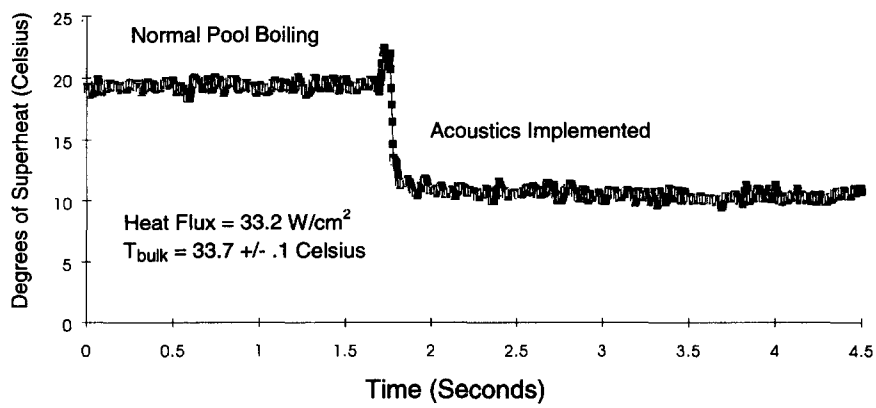

Fig. 5. The effects of an acoustic sound field on pool boiling in a 1 g environment.

increase when the heater was placed at the acoustic pressure antinode. The minimum increase in heat transfer occurred when the heater was at the acoustic pressure node. The augmentation of heat transfer when the heater was placed at positions other than the pressure node and antinode is not presented because the data become quite messy. However, all other acoustic-heat transfer data fall between the heat transfer data with acoustics when the heater was positioned at the pressure node and antinode. In fact, when the heater was placed anywhere within the sound field (except close to the pressure node) the heat transfer approached that corresponding to the heater positioned at the antinode. These results may not directly apply to other fluids. If another fluid is used that requires a higher pressure amplitude to create cavitation, the effects of dynamic bubble levitation and cavitation may be changed which might give different heat transfer results. The highest augmentation to the heat transfer may then occur when the heater is positioned halfway between the pressure node and antinode where the acoustic force is the highest.

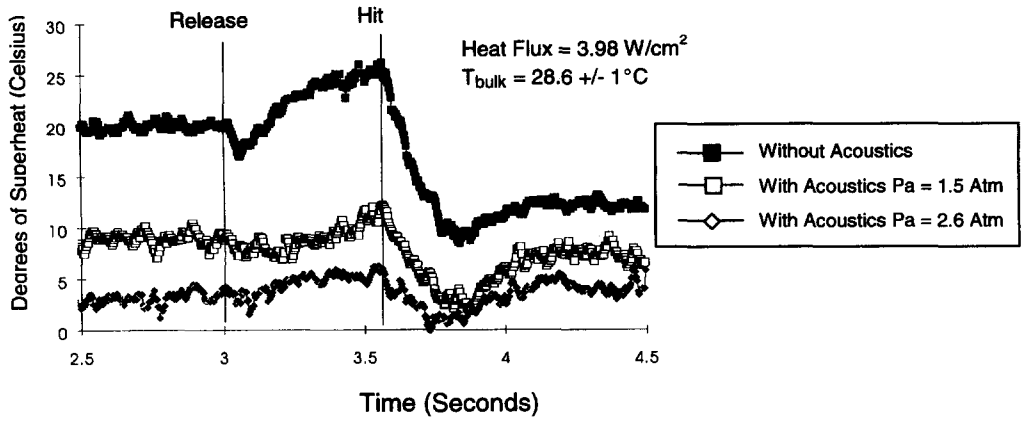

Fig. 6. Pool boiling in terrestrial and microgravity environment at acoustic antinode.

Table 1. Summary of results

Case	T_{sub} (°C)	q (W cm^{-2})	$T_{sup,o}-T_{sup,a}$ (°C) terrestrial G.	h_a/h_o terrestrial G.	$T_{sup,o}-T_{sup,a}$ (°C) microgravity	h_a/h_o microgravity
1	20.8	4.83	5.0	3.51	N/A	N/A
2	20.8	33.2	8.9	1.80	N/A	N/A
3	20.8	77.7	145	1.23	N/A	N/A
4	25.9	3.98	15.7	4.94	18.5	4.79
5	25.9	28.6	7.21	1.27	8.06	1.30
6	24.8	46.4	258	1.72	398	1.97

As vapor bubbles were created at the pressure antinode, bubbles smaller than the resonance size coalesced into bubbles that were larger than the resonance size. Bubbles larger than the resonance size were then driven toward the pressure nodes. As more and more bubbles coalesced at the pressure node the buoyancy force became larger than the acoustic force. The bubbles then rose vertically to the fluid surface.

7.1.2. *Acoustic pressure amplitude.* Wong and Chong [1] found that below a certain acoustic pressure amplitude the effects of acoustics on the heat transfer were negligible. This pressure level is called the critical sound pressure (CSP). This pressure level was found to be equivalent to the cavitation threshold as noted in [1]. The saturation temperature for FC-72 and H_2O are approximately 54 and 100°C, respectively. Thus, a higher acoustic pressure amplitude can be transmitted through water than FC-72 without reaching cavitation. The pressure amplitude needed to levitate a vapor bubble in FC-72 is well within the cavitation zone. However, the pressure needed to levitate a vapor bubble in water is well below the cavitation zone. The CSP for a fluid such as water may be different because the effect of bubble levitation and movement by the acoustic radiation pressure will occur before cavitation. Thus, the effects of cavitation and dynamic bubble levitation on pool boiling should be analyzed separately. This cannot be done when using FC-72 as the experimental fluid.

As the acoustic pressure amplitude is increased the augmentation of heat transfer is also increased (Fig. 6). However, as the pressure level rose well into the cavitation zone, the pressure distribution in the fluid chamber became distorted. Attentuation of the sound field by the cavitation bubbles also became significant. The fluid and the resonator continued to decouple as the sound pressure level was increased beyond the cavitation threshold. This is attributed to the large amounts of vapor being created from the cavitation and boiling process. Therefore, increasing the acoustic pressure within the medium beyond a certain point becomes useless. This sound pressure level was never reached in the current experiments.

The erratic dancing of vapor bubbles due to high acoustic pressures was observed. The dancing behavior was similar to that described by Crum and Eller [15]. This pressure amplitude was different from the pressure at which cavitation started but was very close. With a fluid that has a higher cavitation threshold, this erratic dancing could also theoretically improve heat transfer, even though the fluid is not cavitating.

The calibration of the hydrophone was based upon a linear relation between voltage input to the res-

onator and the voltage output of the hydrophone. However, once the acoustic pressure was high enough to cause cavitation the relationship between the hydrophone and the resonator became nonlinear. Cavitation can occur with a pressure drop of just 0.565 bar (8.19 psi). This pressure value was found by subtracting the saturation pressure corresponding to the bulk temperature of the experiment at 30°C ($P_{sat} = 0.365$ bar) from an atmospheric pressure of 0.93 bar. The fluid could then be boiled at 30°C if the pressure were lowered by 0.565 bar. Therefore, the acoustic pressure amplitude noted in the experiment is not an exact value but only an approximation. The pressure drop of 0.565 bar is rather conservative because the fluid will not homogeneously boil until it is superheated sufficiently. Cavitation was not observed with the unaided eye until the acoustic pressure amplitude reached 1.5 atm gauge.

7.1.3. *Heat flux.* Acoustics had the largest effect on the boiling curve at the inception of boiling and close to burnout (Fig. 3). The temperature of the heater surface dropped by approximately 10°C at the inception of boiling in a sound field. At larger heat fluxes (77.7 W cm^{-2}) the surface temperature dropped 145°C (Case 3 in Table 1). The effects of acoustics on the boiling system diminished in the regime of vapor slugs and columns. In fact acoustics has been reported to have negligible effect on the boiling heat transfer in this heat flux regime [1].

7.2. *Microgravity experiment*

7.2.1. *Heater position.* The effect of acoustics on vapor bubbles in pool boiling is shown in Figs. 7 and 8. When the heater is placed at the acoustic pressure antinode the vapor bubbles were driven toward the pressure node. Only a few bubbles were seen along the heater surface. The vapor was created so fast that the acoustic field could not pull the vapor off the heater fast enough. Larger bubbles were also seen attached to the heater for longer periods of time as the heat flux was increased. These large bubbles attached to the heater were elongated in the direction of the pressure nodes caused by the radiation pressure.

When the heater was located at the acoustic pressure node the bubbles were levitated around the heater. The vapor bubbles varied in size and they were not equally spaced along the heater.

7.2.2. *Acoustic pressure amplitude.* The effects of the pressure amplitude are seen in Fig. 6. For an acoustic pressure amplitude of 1.5 atm gauge and a heat flux of 3.98 W cm^{-2} the surface temperature of the heater dropped by approximately 10°C. When the pressure amplitude was increased to 2.6 atm gauge the overall surface temperature drop was approximately 17°C. The ratio of acoustic pressure amplitude to heater temperature drop for each of the two previously mentioned cases is approximately 6.6°C/(atm). However, once the attentuation of sound becomes dominant, further increases of power to the resonator will produce a lower value for the pressure/temperature relationship.

7.2.3. *Heat flux.* When the acoustic pressure amplitude was zero the pool boiling results were similar to those presented by Straub [3]. At a heat flux of 3.98 W cm^{-2} (Fig. 7) only a few vapor bubbles were created along the heater. These vapor bubbles were seen growing on all sides of the heater without vertical movement. At a heat flux of 24 W cm^{-2} (Fig. 8) the vapor bubbles were evenly distributed along the heater.

The heat transfer had the largest augmentation at a heat flux of 46.4 W cm^{-2} with acoustics present. The surface temperature dropped approximately 258°C (Case 6 in Table 1) in microgravity. However, the surface temperature was not stabilized as time progressed, but continued to increase. Once the experiment returned to terrestrial gravity the temperature dropped and then slowly rose back to its initial predrop temperature. A changing surface temperature during microgravity was also observed at 3.98 W cm^{-2}. The heat transfer also increased at the lower heat fluxes of 3.98 and 24 W cm^{-2} but was not as high. At a heat flux of 24 W cm^{-2} a stable surface temperature was observed during microgravity and the temperature did not drop suddenly as the experiment returned to terrestrial gravity.

7.3. *Degassed fluid*

Degassing the fluid before each experiment is very important [16]. If air is present in the system, the boiling curve will shift during the experiment based on the changing air content. Inception of boiling will occur at reduced pressures and pseudocavitation will be present.

7.4. *Acoustic and heat transfer phenomena in both terrestrial gravity and microgravity*

The effects of cavitation on the surface temperature are seen especially in the heat transfer data in Figs. 5 and 6. At low heat fluxes the surface temperature of the heater was going through well defined oscillations. But as the heat flux increased (Fig. 5) these oscillations are subdued and not as noticeable. At lower heat fluxes, cavitation of the fluid was dominant in creating bubbles compared to the heater. The effects of cavitation and acoustic streaming are seen from the images in Figs. 7 and 8. Cavitation breaks up the vapor bubbles created by the heater into smaller bubbles (if the heater is not positioned at the pressure node). These bubbles dance around in a wild motion and traverse about in the fluid chamber. They finally coalesce at the pressure node. The violent creation and motion of the cavitation bubbles on and around the heater creates more nucleation sites and more vapor embryos. Acoustic streaming and cavitation also removes the thermal overshoot that is normally found at the inception of boiling (Fig. 5). In fact the actual point at which boiling on the heater begins cannot be determined from video footage or from the heat transfer data.

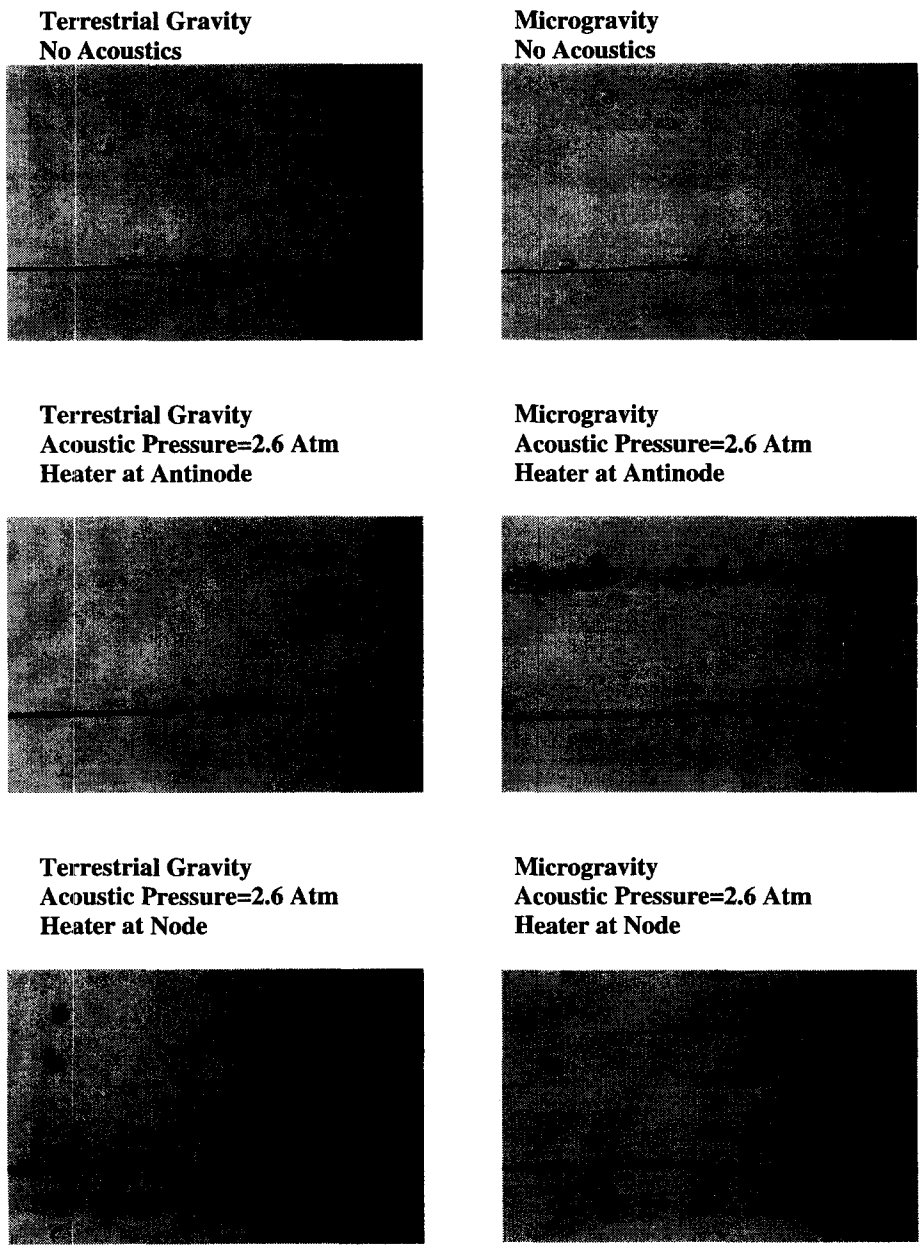

Fig. 7. Visualization of pool boiling from a platinum wire heater with heat flux = 3.98 W cm^{-2} and $T_{bulk} = 28.6 \pm 1°C$.

At higher heat fluxes the amount and size of the vapor bubbles were increased and acoustic cavitation did not dominate. The sound field especially in the vicinity of the heater wire becomes heavily attenuated by vapor. However, the effects of cavitation and acoustic streaming were not totally lost. From visual observation (Fig. 8) it would appear that the fluid was affected by the sound field even at higher heat fluxes. The vapor that normally encapsulates the heater at higher heat fluxes was not stable in the presence of an acoustic sound field. Some of the bubbles were torn off the heater, while others were firmly attached to the heater by surface tension, creating small sections of vapor blanket along the heater. The sections with vapor blanket around the heater were periodically exposed to the fluid which momentarily rewetted the heater surface. Acoustic streaming also aided in carrying more of the subcooled liquid toward the heater. These mechanisms feed the evaporation and condensation processes of the vapor blanket which increased the heat transfer and raised the maximum heat flux.

7.5. *Summary of acoustics results*

The data acquired in Figs. 5 and 6 and other cases of different fluxes are summarized in Table 1. Columns

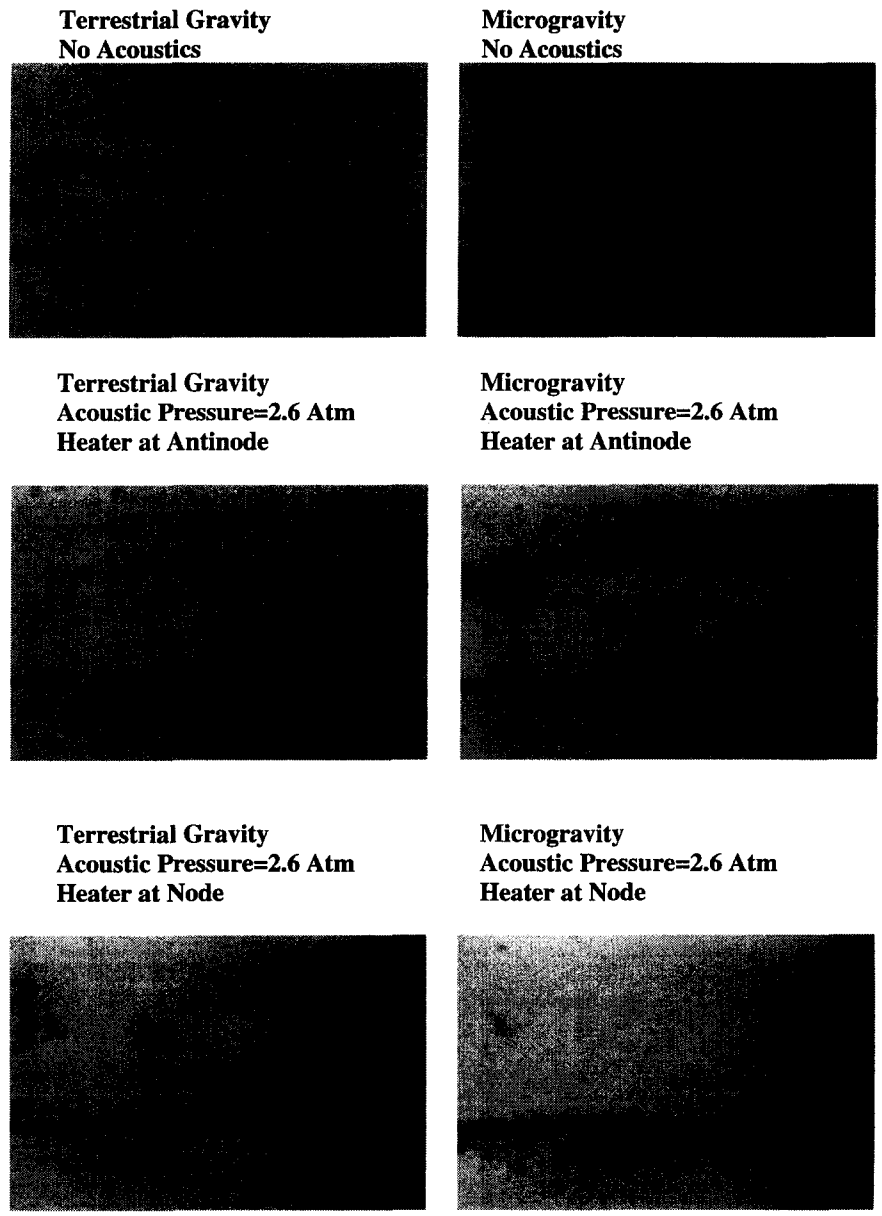

Fig. 8. Visualization of pool boiling from a platinum wire heater with heat flux 24 W cm^{-2} and $T_{bulk} = 28.5 \pm 2°C$.

4 and 6 represent the change in degrees of superheat for the heater when going from pool boiling without acoustics to pool boiling with acoustics. Columns 5 and 7 represent the augmentation of the HTC when using acoustics. The largest increase in the heat transfer occurred at low heat fluxes of 3.98 and 4.83 W cm^{-2} while, the largest temperature difference occurred at the higher heat fluxes of 46.4 and 77.7 W cm^{-2}. This shows the importance of looking at the heat transfer and not just the change in the average surface temperature of the heater.

8. CONCLUSION

The main purpose of this research was to find out if an acoustic field could sustain nucleate pool boiling in microgravity. A pool boiling–acoustic system with a platinum wire heater was designed and constructed to perform experiments in both terrestrial and microgravity conditions. The microgravity experiments were performed in drop towers.

The acoustic force was shown to be strong enough to overcome the terrestrial buoyancy force of an air

bubble in water. The acoustic force appeared to be a promising means of removing vapor from a wire heater in pool boiling during microgravity.

The experiments conducted under terrestrial gravity showed that acoustics can increase the heat transfer under the right pool boiling–acoustic conditions. The highest augmentation of the heat transfer occurred at the inception of boiling. While, at a heat flux of 77.7 W cm^{-2} the average surface temperature of the heater dropped by 145°C. The effects of acoustics on the heat transfer increased as the heat flux went from the conduction regime to the inception of boiling. At the inception of boiling the heat transfer increased by an order of magnitude. However, as the heat flux was increased past the inception of boiling the effects of acoustics on the heat transfer decreased. Once pool boiling extended into the film boiling regime the effects of acoustics were dramatic, the average surface temperature of the heater dropped by over 140°C. It was also shown that when the heater was placed at the acoustic pressure antinode and augmentation of the heat transfer was higher than any other position within the sound field. Degassing the fluid was shown to be a necessity to acquire consistent heat transfer curves.

The pool boiling experiments conducted in microgravity proved that acoustics could move vapor bubbles from the vicinity of the heater. Four different heat fluxes were tried 3.98, 24, 36.4, and 46.4 W cm^{-2}. Under all four heat fluxes the heat transfer increased. Similar to the results in terrestrial gravity the highest augmentation of the heat transfer occurred at a heat flux close to the inception of boiling (3.98 W cm^{-2}) while, at a heat flux of 46.4 W cm^{-2} the average surface temperature of the heater dropped by over 350°C.

For pool boiling in terrestrial conditions or under microgravity, several different acoustic mechanisms were observed: cavitation, streaming, erratic dancing of vapor bubbles, and dynamic bubble levitation. These effects were increased, as the pressure amplitude was raised. Thus, as the motion of vapor bubbles increased so did the heat transfer. In microgravity, the heat transfer data from the heater and the pressure node were inconclusive and further testing is required. The effects of acoustics upon the pool boiling process appeared to aid in heat transfer processes because of the following observations:

1. Vapor bubble movement from the pressure antinode to the pressure node was observed.
2. Film boiling reverted back to nucleate boiling by the perturbation of the vapor blanket and the continual rewetting of the heater surface.
3. Acoustic feeding brought liquid to the heater surface and its surroundings to enhance the evaporation–condensation process.
4. More nucleation sites and vapor embryos were created at lower heat fluxes.
5. Good fluid circulation was found at all heat fluxes.

Acknowledgements—The research was supported by NASA Grant NAG3-1387. Dr Fran Chiaramonte was the project monitor, who provided constant support.

REFERENCES

1. Wong, S. A. and Chon, W. Y., Effects of ultrasonic vibrations on heat transfer to liquids by natural convection and by boiling. *AIChE Journal*, 1969, **15**, 281–288.
2. Iida, Y. and Tsutsui, K., Effects of ultrasonic waves on natural convection, nucleate boiling, and film boiling heat transfer from a wire to a saturated liquid. *Experimental Thermal and Fluid Science*, 1992, **5**, 108–115.
3. Straub, J., Zell, M. and Vogel, B., Pool boiling in a reduced gravity field. *Proceedings of International Heat Transfer Conference*, 1990, pp. 35–57.
4. Eastman, R. E., Dynamics of bubble departure. *AIAA 19th Thermophysics Conference*, Paper 84-1707, 1984.
5. Weinzierl, A. and Straub, J., Nucleate pool boiling in microgravity environment. *Proceedings of the Seventh International Heat Transfer Conference*, Vol. 4. Hemisphere, Munich, 1982, pp. 21–27.
6. Park, K. A. and Bergles, A. E., Ultrasonic enhancement of saturated and subcooled pool boiling. *International Journal of Heat and Mass Transfer*, 1988, **31**, 664–667.
7. Marston, P. L., Evaporation–condensation resonance frequency of oscillating vapor bubbles. *J. Acoust. Soc. Am.*, 1979, **66**, 664–667.
8. Asaki, T. J. and Marston, P. L., Acoustic radiation force on a bubble driven above resonance. *J. Acoust. Soc. Am.*, 1994, **96**, 3096–3099.
9. Crum, L. A., Acoustic force on a liquid droplet in an acoustic stationary wave. *J. Acoust. Soc. Am.*, 1971, **50**, 157–163.
10. Eller, A., Force on a bubble in a standing acoustic wave. *J. Acoust. Soc. Am.*, 1968, **43**, 170–171.
11. Sitter, J. S., Acoustic driven nucleate pool boiling heat transfer in terrestrial and microgravity environments. M.S. thesis, Washington State University, Pullman, WA, 1995.
12. Cooper, M. G., Judd, A. M. and Pike, R. A., Shape and departure of single bubbles growing at a wall. *Proceedings of the Sixth International Heat Transfer Conference*, 1978, pp. 115–120.
13. Incropera, F. P. and De Witt, D. P., *Introduction of Heat Transfer*, 3rd edn. John Wiley and Sons, 1990, p. 457.
14. Carey, V. P., *Liquid–Vapor Phase-Change Phenomena*. Hemisphere Publishing Corporation, 1992.
15. Crum, L. A. and Eller, A., Motion of bubbles in a stationary sound field. *J. Acoust. Soc. Am.*, 1970, **48**, 1123–1132.
16. Hong, Y. S., Ammerman, C. N. and You, S. M., Boiling characteristics of cylindrical heaters in saturated, gas saturated, and pure-subcooled FC-72. *ASME Journal of Heat Transfer*, 1997, **119**, 313–318.